Int. J. Electrochem. Sci., 9 **(2014)** 7540 - 7551

International Journal of
ELECTROCHEMICAL
SCIENCE
www.electrochemsci.org

Free-standing PEDOT:PSS Film as Electrode for the Electrodeposition of Bismuth Telluride and Its Thermoelectric Performance

Qinglin Jiang[†], *Congcong Liu*[†], *Haijun Song, Jingkun Xu*[*], *Daize Mo, Hui Shi, Zhipeng Wang, Fengxing Jiang, Baoyang Lu, and Zhengyou Zhu*

Jiangxi Key Laboratory of Organic Chemistry, Jiangxi Science and Technology Normal University, Nanchang 330013, PR China
[*]E-mail: xujingkun@tsinghua.org.cn
†: These authors contributed equally to this work

Received: 2 September 2014 / *Accepted:* 15 October 2014 / *Published:* 28 October 2014

In the present work, a free-standing poly(3,4-ethylenedioxythiophene): poly(styrenesulfonate) (PEDOT:PSS) film was used as a working electrode to electrodeposit bismuth telluride (Bi_2Te_3) and acted as a part of the prepared sandwich-like structured Bi_2Te_3/PEDOT:PSS/Bi_2Te_3 composite film. Structures and surface morphologies were systematically investigated by the characterizations of cross-section SEM, EDX, FT-IR, and TGA. A relatively low thermal conductivity of 0.169-0.179 W/m/K was obtained, which was beneficial to the enhancement of thermoelectric performance. The electrical conductivity of Bi_2Te_3/PEDOT:PSS/Bi_2Te_3 composite film was determined to be up to 403.5 S/cm. The *ZT* value reached up to be a maximum value of 1.72×10^{-2}. Thus, this technique offers a facile approach to electrodeposit a new generation of materials for more practical applications.

Keywords: PEDOT:PSS electrode; electrodeposition; bismuth telluride; thermoelectric; thermal conductivity

1. INTRODUCTION

Electrodeposition has been proved to be one of the most effective approaches to prepare metallic and compound materials owing to several merits including one-step film formation, easily controlled reaction rate and product output [1]. Generally speaking, experimental conditions such as solvents, concentration of reagents, supporting electrolytes, nature of the electrodes, applied electrical conditions, and temperature could determine the results of electrodeposition in a certain extent. Among them, the electrode is a critical factor since it may affect both the deposition process and properties of

the resulting product [2]. Traditional electrode materials for electrodeposition are generally noble metals (platinum, gold), stainless steel, carbon materials, or optically transparent electrodes such as indium-tin oxide (ITO) [3-7]. Although they are of excellent stability and high conductivity, their respective defects are often accompanied by some factors, including the scarcity of indium, high price of precious metals, and poor mechanical flexibility. Hence, it is of great importance to develop new alternative electrode materials.

The unique features of organics including low cost, light weight, reduced environmental impact, flexibility, processability, structure diversity and fast kinetics provide organic electrode materials many perspective applications [8]. Poly(3,4-ethylenedioxythiophene):poly(styrenesulfonate) (PEDOT:PSS), one of the most useful and commercial conducting polymers, exhibit high stability and enhanced electrical conductivity by post-treatment [9-11]. It has been widely applied as conductive electrode in organic electronics such as field-effect transistors, light-emitting diodes, and solar cells [9-13]. Moreover, Groenendaal *et al*. predicted that PEDOT:PSS was promising to be the next-generation electrode material in the organic electronic field owing to its solution processability, high mechanical flexibility, environmental stability, ease of synthesis, and high electrical conductivity [14]. Recently, our group reported a pure organic PEDOT:PSS film as the working electrode to successfully deposit conducting polymers, providing a facile and general method for the electrodeposition [15].

As an effective thermoelectric (TE) material, bismuth telluride (Bi_2Te_3) has been made fascinating breakthroughs in the practical application, some of which are even reaching the marketplace [16,17]. In general, TE materials are ranked by a figure of merit, *ZT*, which is defined as $ZT = S^2\sigma T/\kappa$, where S, σ, T, and κ are the Seebeck coefficient, electrical conductivity, absolute temperature, and thermal conductivity, respectively [18]. Various methods have been developed for the preparation of Bi_2Te_3, such as sputtering [19], metallorganic chemical vapor deposition (MOCVD) [20], physical vapor deposition (PVD) [21], molecular beam expitaxy (MBE) [22] and electrodeposition [23-25]. Among those techniques, electrodeposition has been widely investigated owing to its certain advantages including cost-effectiveness, rapid deposition rates, large-area coverage, and low deposition temperature [25]. The current methods to obtain Bi_2Te_3 are mainly based on the traditional electrode materials, and PEDOT:PSS film as working electrode for the electrodeposition of Bi_2Te_3 has never been reported.

On the other hand, as a typical organic TE material, Bi_2Te_3 possesses a thermal conductivity of around 1 W/m/K [26], which is against the enhancement of *ZT* value. Conducting polymers intrinsically possess low thermal conductivity typically ranging from 0.08 to 0.60 W/m/K [27]. Especially, PEDOT:PSS displayed a low thermal conductivity of 0.168 W/m/K, making it a promising thermoelectric material [28]. Synthesizing composites combined inorganic TE materials with conducting polymers was considered an effective strategy to reduce the thermal conductivity, thus improving the TE performances [29]. Therefore, considering the advantages of PEDOT:PSS used as working electrode, electrodeposition of Bi_2Te_3 on this PEDOT:PSS electrode may be an effective way for the fabrication of improved TE materials.

In the present work, a PEDOT:PSS film electrode was used to electrodeposit Bi_2Te_3, fabricating a sandwich-like structured Bi_2Te_3/PEDOT:PSS/Bi_2Te_3 composite film. Additional

properties of the as-formed composite films, such as structures and surface morphologies, were also investigated in detail through cross-section SEM, EDX, FT-IR, and TGA.

2. EXPERIMENTAL

2.1 Preparation of PEDOT:PSS films

PEDOT:PSS aqueous solution (CLEVIOS PH1000) was purchased from H.C. Starck and used as received. The concentration of PEDOT:PSS was 1.3% by weight, and the weight ratio of PSS to PEDOT was 2.5. PEDOT:PSS/5 vol.% dimethyl sulfoxide (herein referred to as PEDOT:PSS) solution was drop-cast on the polypropylene (PP) substrate, and dried in vacuum at 80 ^{o}C for 12 h. Then, a free-standing and flexible PEDOT:PSS film was easily obtained by peeling off from the PP substrate.

2.2. Electrolyte solutions

$Bi(NO_3)_3{\cdot}5H_2O$ and TeO_2 were both analytical grade and purchased from Sigma-Aldrich. $Bi(NO_3)_3{\cdot}5H_2O$ was dissolved in 1 M HNO_3 to prepare electrolytes of desired Bi concentration. In order to completely dissolve the TeO_2, concentrated HNO_3 was used and the electrolyte was then diluted to pH 0 measured by the pH meter. Milli-Q water (resistivity 18 MΩ cm) collected from a Barnstead E-pure filtration system was used to prepare all the electrolyte solutions.

2.3. Electrodeposition

All electrochemical experiments were performed at room temperature using a CHI660B electrochemical workstation (Shanghai Chenhua Instrument Company, China) with a scan rate of 25 mV/s. A conventional three-electrode set-up was constructed for the electrodeposition. The free-standing PEDOT:PSS film was used as working electrode placed perpendicularly in the electrolyte solutions. Opposite to the working electrode, a stainless-steel sheet was used as counter electrode and the reference electrode was an Ag/AgCl electrode. Prior to each experiment, the electrolyte solutions were purged with nitrogen gas for 10 min to remove dissolved oxygen. Bi_2Te_3 was electrodeposited by cyclic voltammetry from -0.8 to 1.0 V. By controlling the cycle numbers at 1, 5, 10, and 15, Bi_2Te_3/PEDOT:PSS/$Bi_2Te_3$1, Bi_2Te_3/PEDOT:PSS/$Bi_2Te_3$5, Bi_2Te_3/PEDOT:PSS/$Bi_2Te_3$10, and Bi_2Te_3/PEDOT:PSS/$Bi_2Te_3$15 composite films were obtained, respectively.

2.4. Characterization

The morphologies of the prepared films were investigated by scanning electron microscopy (SEM, ZEISS-SIGMA). The composition of the deposits was obtained using combined energy-dispersive X-ray spectroscopy (EDX). Infrared spectra were recorded using a Bruker Vertex 70

Fourier transform infrared (FT-IR) spectrometer with samples in KBr pellets. Thermogravimetric analysis (TGA) was performed with a Pyris Diamond TG/DTA thermal analyzer (Perkin-Elmer).

Electrical conductivity and Seebeck coefficient were measured with a homemade shielded four-point probe apparatus with a Keithley 2700 Multimeter (Cleveland, OH) and a regulated DC power supply (MCH-303D-II, China) in conjunction with Labview (National Instruments, Austin, TX). Samples were cut into pieces of a rectangular shape and suspended by using a thermal paste between two TE devices used for creating temperature difference. Electrical conductivity was measured by using a current–voltage (IV) sweeping measurement technique with four-point probes after four metal lines were patterned with a silver paint. For the Seebeck coefficient measurement, temperature gradients along the long edge of the sample were measured by two T-type thermocouples. The thermal conductivity was measured by TC3010 (Xi'an, China) using the transient hot wire method.

3. RESULTS AND DISCUSSION

3.1 Electrodeposition of Bi_2Te_3 on the PEDOT:PSS electrode

As shown in Figure 1, the free-standing and flexible PEDOT:PSS film was directly used as working electrode for the electrodeposition of Bi_2Te_3, employing a stainless-steel sheet as the counter electrode, and Ag/AgCl electrode as the reference electrode, respectively. Bi_2Te_3 was simultaneously electrodeposited on both sides of the flexible PEDOT:PSS electrode, forming an interesting Bi_2Te_3/PEDOT:PSS/Bi_2Te_3 sandwich-like structure.

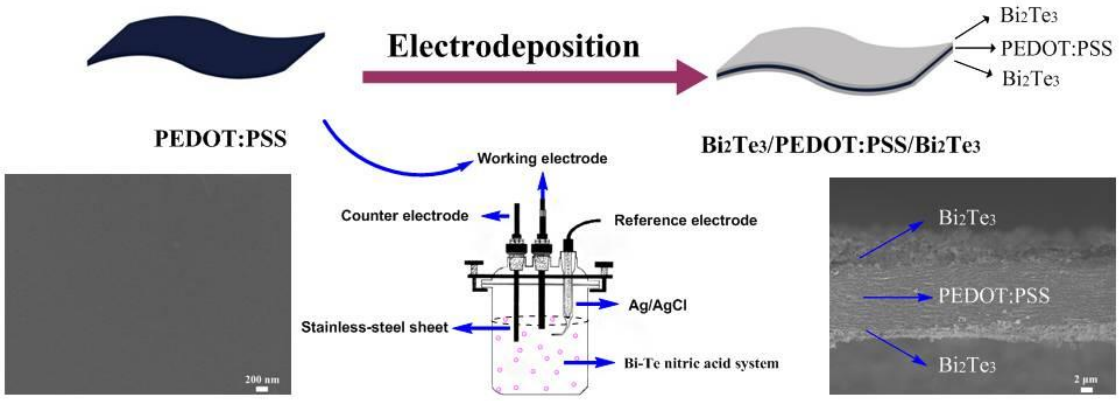

Figure 1. Schematic diagram of Bi_2Te_3 electrodeposited on the flexible PEDOT:PSS electrode. The insets were the SEM images of PEDOT:PSS and the cross-section of Bi_2Te_3/PEDOT:PSS/Bi_2Te_3 film

According to the Pourbaix diagram, bismuth and tellurium can be completely dissolved in 1 M HNO_3 and will exist mainly as Bi^{3+} and $HTeO_2^+$ [30]. The electrochemical behavior of 1 M HNO_3 solutions containing 7.5 mM Bi^{3+} and 10 mM $HTeO_2^+$ was studied by cyclic voltammetry experiments, as shown in Figure 2. The solution concentration ratio was based on the previous studies which

showed that excess Bi in the solution leads to stoichiometric Bi_2Te_3 deposition [31]. During the cathodic scan, the deposition takes place by the electrochemically induced reduction of Bi^{3+} and $HTeO_2^+$. The formula (1) and (2) shows the reaction of Bi^{3+} and $HTeO_2^+$ [32,33]

$$Bi^{3+} + 3e^- \leftrightharpoons Bi(s) \quad (1)$$

$$HTeO_2^+ + 3H^+ + 4e^- \leftrightharpoons Te + 2H_2O \quad (2)$$

It was observed that the reduction peak at a negative potential of -80 mV corresponding to a simultaneous reduction reaction reported as a co-deposition process [34], expressed in the following chemical formula:

$$3HTeO_2^+ + 2Bi^{3+} + 9H^+ + 18e^- \leftrightharpoons Bi_2Te_3(s) + 6H_2O \quad (3)$$

As for the deposition of Te, a two-step mechanism has been proposed [31,35], where $HTeO_2^+$ is first reduced to elemental Te and $HTeO_2^+$ will be directly reduced to unstable H_2Te which reacts with the rest of $HTeO_2^+$ to form elemental Te again. It was suggested consisting of two consecutive reactions as follows [36]:

$$HTeO_2^+ + 5H^+ + 6e^- \leftrightharpoons H_2Te(aq) + 2H_2O \quad (4)$$

$$2H_2Te + HTeO_2^+ \rightarrow 3Te(s) + 2H_2O + H^+ \quad (5)$$

During the anodic scan, H_2Te is likely formed and the extra Te subsequently formed from H_2Te according to formula (5) contributed to the oxidation peak at 0.75 V.

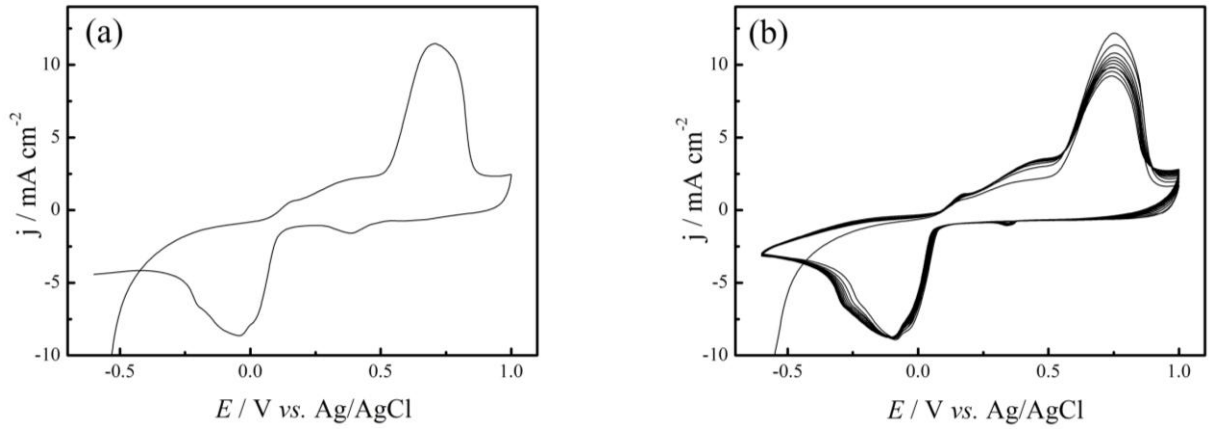

Figure 2. Cyclic voltammogram of Bi_2Te_3 electrodeposited on the PEDOT:PSS electrode for different cycles: (a) 1, (b) 10. Scan rate: 25 mV/s

Figure 3 presents the SEM micrographs and EDX analysis of Bi_2Te_3/PEDOT:PSS/Bi_2Te_3 composite films prepared by different cycle numbers. Initially, the surface of pure PEDOT:PSS electrode was uniform and smooth (Figure 1). However, it changed obviously after the electrodeposition of Bi_2Te_3 for 1 cycle, which was comprised of nanoparticles (Figure 3a). Upon the further deposition, a large number of aggregates composed of Bi_2Te_3 grains were randomly distributed on the PEDOT:PSS working electrode, and the distribution of the Bi_2Te_3 aggregates becomes increasingly dense with the cycles (Figure 3b-c). After 15 cycles of deposition, a compact and continuous film was formed, as shown in Figure 3d. The cross-section SEM image of Bi_2Te_3/PEDOT:PSS/Bi_2Te_3 film clearly showed that Bi_2Te_3 grains were simultaneously deposited on

both sides of the flexible PEDOT:PSS electrode (Figure 1), forming an interesting Bi_2Te_3/PEDOT:PSS/Bi_2Te_3 sandwich-like structure. From the EDX analysis of prepared composite films (Figure 3e), the strong Bi and Te peaks could be easily observed, and the peaks of C and O could be ascribed to the PEDOT:PSS working electrode.

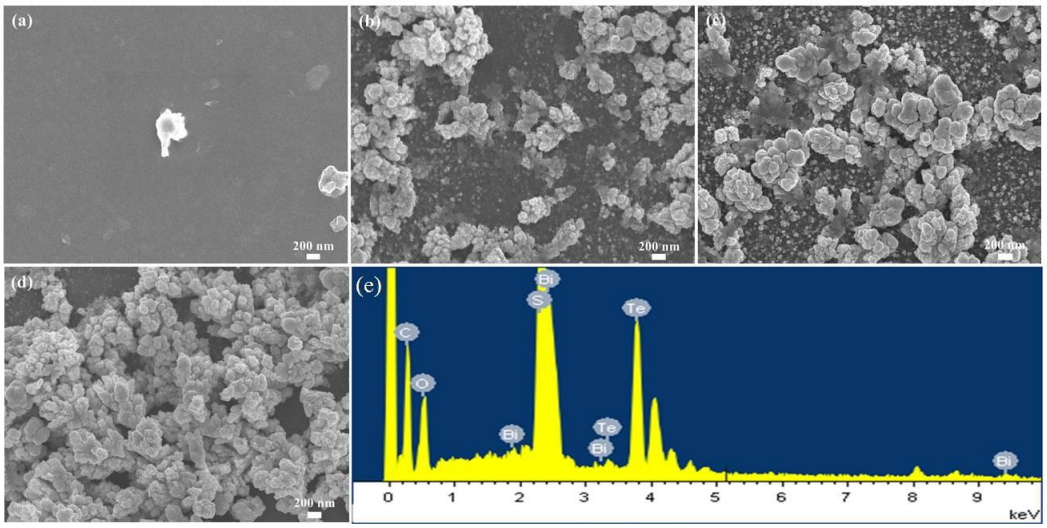

Figure 3. SEM images of Bi_2Te_3 electrodeposited on the PEDOT:PSS electrode for different cycles: (a) 1, (b) 5, (c) 10, (d) 15. (e) EDX analysis of the Bi_2Te_3/PEDOT:PSS/Bi_2Te_3 composite films

Figure 4 shows the FT-IR spectra of PEDOT:PSS electrode and Bi_2Te_3/PEDOT:PSS/Bi_2Te_3 composite films. Obviously, all samples display characteristic peaks of PEDOT:PSS (Figure 4a-e), which was in consistent with previously reported literature [37]. The vibrations at 1316 and 1520 cm^{-1} were caused by the C-C and C=C stretching of the quinoidal structure and the ring stretching of the thiophene ring of the PEDOT chains [15]. The absorption peak at 1203 cm^{-1} of pristine PEDOT: PSS, corresponding to the SO_3H group of PSS [38]. The band at about 831 cm^{-1} was related to the C−S bond vibration in the thiophene ring [39]. In addition, the Bi_2Te_3/PEDOT:PSS/Bi_2Te_3 composite films showed a strong peak at 1384 cm^{-1} (Figure 4b-e), corresponding to the characteristic peaks of the Bi_2Te_3 (inset of Figure 4), which was direct proof of the composites of Bi_2Te_3 and PEDOT:PSS.

As shown in Figure 5, the thermal stability of PEDOT:PSS electrode and Bi_2Te_3/PEDOT:PSS/Bi_2Te_3 composite films were investigated by thermogravimetric analytical experiments under a nitrogen stream at the heating rate of 10 K min^{-1}. It was clearly observed that there were three-step weight losses for all the samples. Initially, the films underwent a small weight decrease (about 19.05% for PEDOT:PSS electrode, 13.65% for Bi_2Te_3/PEDOT:PSS/$Bi_2Te_3$10 and 11.12% for Bi_2Te_3/PEDOT:PSS/$Bi_2Te_3$15) at relatively low temperature (from 290 K to 506 K), which may be attributed to moisture evaporation in the films [40]. With the gradual increasing of temperature, a prominent weight loss step about 34.87% for PEDOT:PSS electrode at 506 K < T < 715 K, which was essentially due to the oxidizing decomposition of the skeletal PEDOT and/or PSS backbone chain structures [41]. The composite films also displayed the same as the PEDOT:PSS electrode, such as the weight loss about 25.17% for the Bi_2Te_3/PEDOT:PSS/$Bi_2Te_3$15 composite film

at 506 K < *T* < 685 K. The degradation rate of Bi_2Te_3/PEDOT:PSS/$Bi_2Te_3$10 and Bi_2Te_3/PEDOT:PSS/$Bi_2Te_3$15 was slower than that of pure PEDOT:PSS electrode, and the remaining content of them were all higher than it. These results clearly indicated that Bi_2Te_3 was electrodeposited on the PEDOT: PSS electrode successfully, and Bi_2Te_3/PEDOT:PSS/Bi_2Te_3 sandwich-like composite films showed better thermal stability when compared with the PEDOT:PSS electrode.

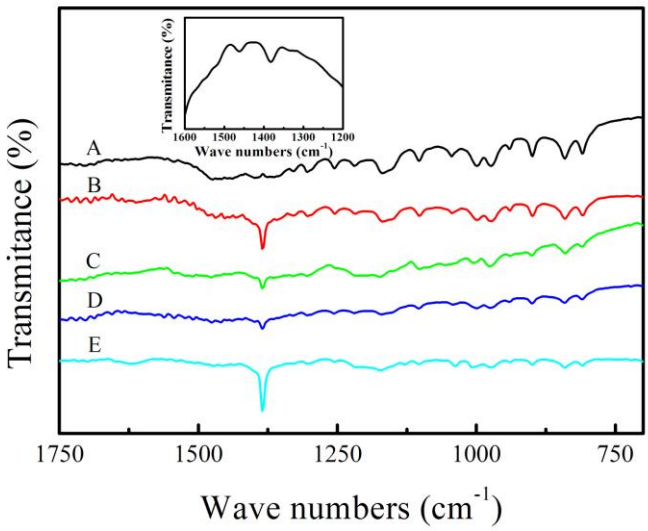

Figure 4. FT-IR spectra of (A) PEDOT:PSS electrode and Bi_2Te_3 electrodeposited on the PEDOT:PSS electrode for different cycles: (B) 1, (C) 5, (D) 10, (E) 15. Inset was the FT-IR spectra of Bi_2Te_3

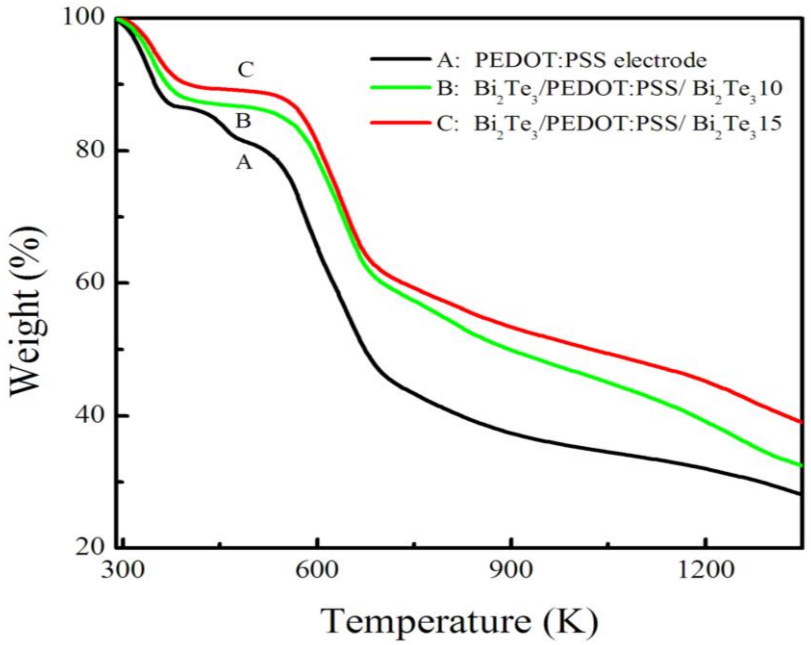

Figure 5. TGA curves of (A) PEDOT:PSS electrode and Bi_2Te_3 electrodeposited on the PEDOT:PSS electrode for different cycles: (B) 10, (C) 15

3.2 TE performance of the Bi_2Te_3/PEDOT:PSS/Bi_2Te_3 composite films

A high-performance TE material requires a low thermal conductivity to prevent thermal shorting. However, inorganic TE materials possess higher thermal conductivity when compared with conducting polymer TE materials, which was against the enhancement of *ZT* value. By the synthesis of composites, reduced thermal conductivity (0.22-0.56 W/m/K) was obtained in the PEDOT:PSS/inorganic composite materials [42-45], but still higher than that (0.17 W/m/K) of PEDOT:PSS [28]. Herein, the thermal conductivity of PEDOT:PSS electrode and Bi_2Te_3/PEDOT:PSS/Bi_2Te_3 composite films was studied, as shown in Table 1. The PEDOT:PSS electrode showed a low thermal conductivity of 0.168 W/m/K. Encouragingly, with the electrodeposition of Bi_2Te_3, the Bi_2Te_3/PEDOT:PSS/Bi_2Te_3 composite films did not show remarkably increased thermal conductivity compared with the PEDOT:PSS electrode, retaining a low value of 0.169-0.179 W/m/K. It was worth noting that this value was much lower than that of Bi_2Te_3 (1 W/m/K) [26] and previously reported PEDOT:PSS/Bi_2Te_3 (0.560 W/m/K) composite materials [45].

Table 1. Thermal conductivity of PEDOT:PSS electrode and Bi_2Te_3/PEDOT:PSS/Bi_2Te_3 composite films in this work and the previously reported value of Bi_2Te_3 and PEDOT:PSS/Bi_2Te_3 composite film

Sample	Thermal Conductivity [W/m/K]	Refs.
PEDOT:PSS electrode	0.168	This work
Bi_2Te_3/PEDOT:PSS/$Bi_2Te_3$1	0.176	This work
Bi_2Te_3/PEDOT:PSS/$Bi_2Te_3$5	0.179	This work
Bi_2Te_3/PEDOT:PSS/$Bi_2Te_3$10	0.169	This work
Bi_2Te_3/PEDOT:PSS/ $Bi_2Te_3$15	0.172	This work
Bi_2Te_3	1.000	[26]
PEDOT:PSS/Bi_2Te_3	0.560	[45]

Such a low thermal conductivity is mainly attributed to the poor thermal conductivity of the PEDOT:PSS phase and phonon scattering from the substantial grain boundaries provided by the Bi_2Te_3 particles and the phase boundaries between the PEDOT:PSS and Bi_2Te_3 phases [46]. Therefore, this approach may offer a simple way to reduce the thermal conductivity of some materials, and thus improved TE properties might be obtained.

The two main parameters related to the TE performance, namely the electrical conductivity and Seebeck coefficient, were also investigated. As for the PEDOT:PSS electrode, it possesses an electrical conductivity of 280.5 S/cm and a Seebeck coefficient of 15.2 μV/K. Figure 6 presents the room-

temperature electrical conductivity and Seebeck coefficient of Bi_2Te_3/PEDOT:PSS/Bi_2Te_3 composite films as a function of the cycle numbers. It was found that the Bi_2Te_3/PEDOT:PSS/$Bi_2Te_3$1 displayed an electrical conductivity of 308.6 S/cm, and the electrical conductivity ascended with the increasing cycle numbers.

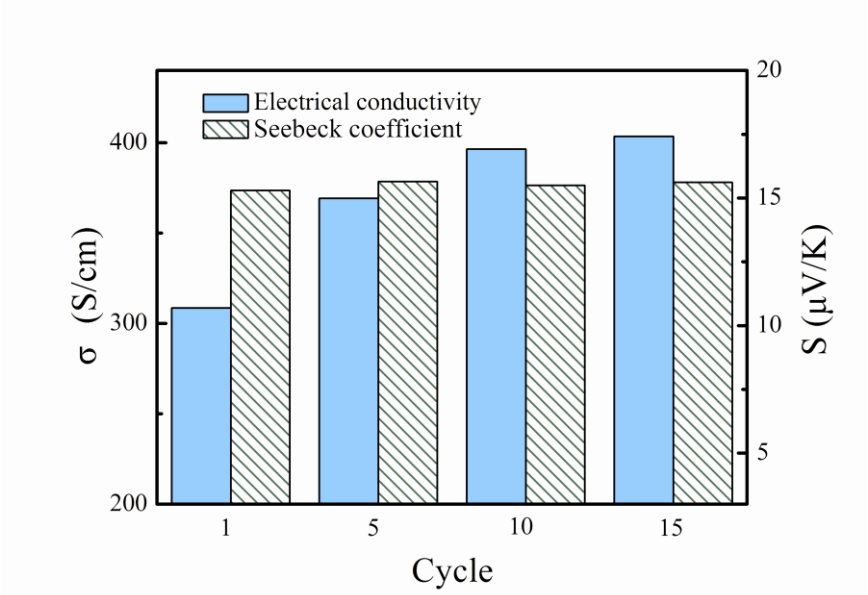

Figure 6. Electrical conductivity and Seebeck coefficient of Bi_2Te_3/PEDOT:PSS/Bi_2Te_3 composite films as a function of cycle numbers

The highest value reached to 403.5 S/cm after 15 cycles. According to the previous work, the Bi_2Te_3 nanocrystals pellet [47] and Bi_2Te_3 nanoparticles [48] exhibited the electrical conductivity of 30 S/cm and 49.6 S/cm. Thus, the electrical conductivity of Bi_2Te_3/PEDOT:PSS/Bi_2Te_3 composite film in our present work was enhanced and preferable.

Seebeck coefficient is an intrinsic electronic transport property, defined as $S = \Delta V/\Delta T$, where ΔV and ΔT are the voltage drops across the material and the temperature gradient along the voltage drop. It is determined by setting up a temperature gradient of ΔT = 5 K and measuring the output voltage between both ends of sample. As shown in Fig. 6, the Seebeck coefficient of these simples were positive, indicating the dominant contribution of hole carriers [49]. At 300 K, Bi_2Te_3/PEDOT:PSS/$Bi_2Te_3$1 showed a Seebeck coefficient of 15.3 μV/K. With the increasing of cycle numbers, the Seebeck coefficient fluctuated within a small range of 15.3-15.7 μV/K, whereas the electrical conductivity was enhanced. It is believed that Seebeck coefficient measures the entropy transported with a charge carrier as it moves, divided by the carrier's charge [50]. This entropy difference can be changed by the electrical and thermal conductivity. When the electrical conductivity increased, it could facilitate charge diffusion between the high- and low-temperature surfaces, causing an increase of the Seebeck effect. However, increasing the electrical conductivity could also lead to an increase in the electron component of thermal conductivity through the Wiedemann-Franz law $\kappa_{electron}/\sigma T = C$, where $\kappa_{electron}$ is the electron component of the thermal conductivity and C is a constant [51]. This tends to decrease the entropy difference driving the charge diffusion in the development of the Seebeck effect. Therefore, increasing the electrical conductivity can cause two competing

outcomes: increasing and decreasing the Seebeck effect. It is believed that here the two outcomes are mutually coordinated in Bi_2Te_3/PEDOT:PSS/Bi_2Te_3 composite films, so that the values of Seebeck coefficient fluctuated smoothly in a tiny range.

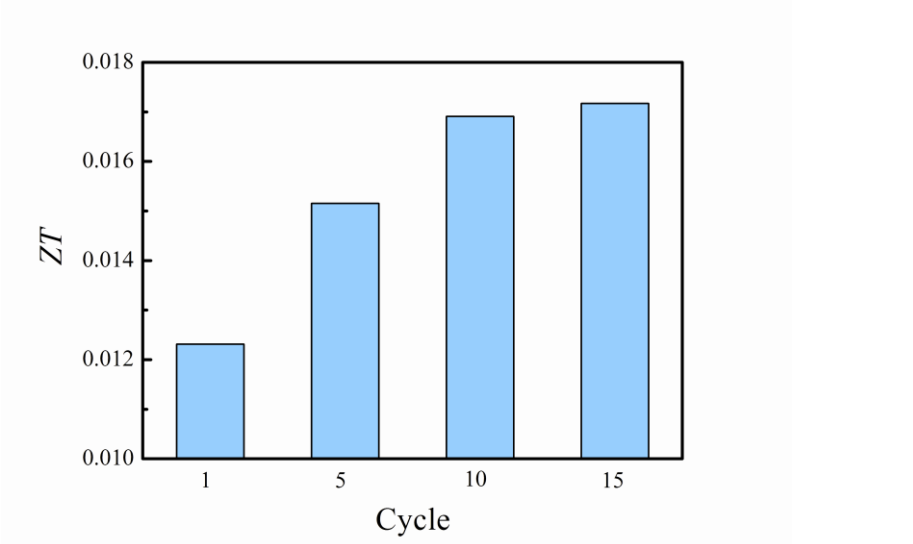

Figure 7. *ZT* value of Bi_2Te_3/PEDOT:PSS/Bi_2Te_3 composite films as a function of cycle numbers

According to the above experimental result, the *ZT* value of Bi_2Te_3/PEDOT:PSS/Bi_2Te_3 composite film was obtained, as shown in Figure 7. As the increase of cycle numbers, the *ZT* value of Bi_2Te_3/PEDOT:PSS/Bi_2Te_3 composite film was enhanced. After 15 cycles, the value could be up to 1.72×10^{-2}. It is clear that remarkably enhanced *ZT* value have been accomplished by Bi_2Te_3/PEDOT:PSS/Bi_2Te_3 composite films, owing to the low thermal conductivity together with the high electrical conductivity and stable Seebeck coefficient. Although their performance are still inferior to those of conventional inorganic thermoelectric materials, we expect that some thermoelectric composites with high performances could be achieved using a similar method. Because of the square dependence of the *ZT* value on the Seebeck coefficient, further improvement will be expected to occur with the improvement of the Seebeck coefficient. For instance, we could replace Bi_2Te_3 with lead telluride (PbTe), graphene, and carbon nanotubes (CNTs).

4. CONCLUSIONS

In conclusion, a novel working electrode of PEDOT:PSS film was raised for the electrodeposition of Bi_2Te_3, and a sandwich-like structured Bi_2Te_3/PEDOT:PSS/Bi_2Te_3 composite film was formed. The structures and surface morphologies were systematically investigated. The composite films exhibited TE properties of a favourable low thermal conductivity (0.169-0.179 W/m/K) and a high electrical conductivity (403.5 S/cm), and their *ZT* value reached a maximum of 1.72×10^{-2}. Most importantly, this approach may provide a facile and general method for the electrodeposition of materials with better performance for a wider array of application.

ACKNOWLEDGEMENTS
This work was supported by National Natural Science Foundation of China (51303073 & 51203070), Jiangxi Provincial Department of Education (YC2013-S270 & GJJ13565), and Jiangxi Provincial Department of Science and Technology (20122BAB216011), Training Plan for the Main Subject of Academic Leaders of Jiangxi Province.

References

1. W. Chen and G. Xue, *Prog. Polym. Sci.*, 30 (2005) 783.
2. J. Roncali, *Chem. Rev.*, 92 (1992) 711.
3. G. M. Nie, T. Cai, J. K. Xu and S. S. Zhang, *Electrochem. Commun.*, 10 (2008) 186.
4. Y. Y. Yao, Y. P. Wen, L. Zhang, J. K. Xu, Z. F. Wang and X. M. Duan, *Int. J. Electrochem Sci.*, 8 (2013) 9348.
5. G. Q. Shi, S. Jin, G. Xue and G. Li, *Science*, 267 (1995) 994.
6. K. P. Prathish, R. C. Carvalho and C. M. A. Brett, *Electrochem. Commun.*, 44 (2014) 8.
7. T. P. Huynh, P. Pieta, F. D'Souza and W. Kutner, *Anal. Chem.*, 85 (2013) 8304.
8. Z. P. Song and H. S. Zhou, *Energy Environ. Sci.*, 6 (2013) 2280.
9. D. Alemu, H. Y. Wei, K. C. Ho and C. W. Chu, *Energy Environ. Sci.*, 5 (2012) 9662.
10. H. Sirringhaus, T. Kawase, R. H. Friend, T. Shimoda, M. Inbasekaran, W. Wu and E. P. Woo, *Science*, 290 (2000) 2123.
11. Y. Du, S. Z. Shen, K. F. Cai and P. S. Casey, *Prog. Polym. Sci*., 37 (2012) 820.
12. Kim, S. Kee, S. H. Lee, B. H. Lee, Y. H. Kahng, Y. R. Jo, B. J. Kim and K. Lee, *Adv. Mater.*, 26 (2014) 2268.
13. J. Y. Ouyang, *ACS Appl. Mater. Interfaces*, 5 (2013) 13082.
14. L. Groenendaal, F. Jonas, D. Freitag, H. Pielartzik and J. R. Reynolds, *Adv. Mater*., 12 (2000) 481.
15. H. Shi, C. C. Liu, J. K. Xu, H. J. Song, B. Y. Lu, F. X. Jiang, W. Q. Zhou, G. Zhang and Q. L. Jiang, *ACS Appl. Mater. Interfaces*, 5 (2013) 12811.
16. D. M. Rowe, CRC Handbook of Thermoelectrics, CRC press, (1995), Chp. 3.
17. R. K. Willardson, A. C. Beer and T. M. Tritt, Recent Trends in Thermoelectric Materials Research, Semiconductors and Semimetals, vol. 69, 2001, Chp. 1.
18. H. J. Goldsmid, Thermoelectric Refrigeration, Plenum, New York, (1964).
19. Y. H. Shing, Y. Chang, A. Mirshafii, L. Hayashi, S. S. Roberts, J. Y. Josefowicz and N. Tran, *J. Vac. Sci. Technol. A*, 1 (1983) 503.
20. R. Venkatasubramanian, T. Colpitts, B. O'Quinn, S. Liu, N. E. Masry and M. Lamvik, *Appl. Phys. Lett.*, 75 (1999) 1104.
21. H. Zoos, D. M. Rowe and G. Min, *J. Cryst. Growth*, 222 (2001) 82.
22. T. C. Harman, P. J. Taylor, D. L. Spears and M. P. Walsh, *J. Electron. Mater.*, 29 (2000) L1.
23. M. Takahashi, Y. Katou, K. Nagata and S. Furuta, *Thin Solid Films*, 240 (1994) 70.
24. W. L. Wang, C. C. Wan and Y. Y. Wang, *Electrochim. Acta*, 52 (2007) 6502.
25. D. W. Liu and J. F. Li, *J. Electrochem. Soc.*, 155 (2008) D493.
26. F. F. Kong, C. C. Liu, J. K. Xu, Y. Huang, J. M. Wang and Z. Sun, *J. Electron. Mater.*, 41 (2012) 2431.
27. M. Hu, D. M. Yu and J. B. Wei, *Polym. Test.*, 26 (2007) 333.
28. F. X. Jiang, J. K. Xu, B. Y. Lu, Y. Xie, R. J. Huang and L. F. Li, *Chin. Phys. Lett.*, 25 (2008) 2202.
29. Y. Du, S. Z. Shen, K. F. Cai and P. S. Casey, *Prog. Polym. Sci.*, 37 (2012) 820.
30. M. Pourbaix, Atlas d' Equilibres Electrochimiques, Gauthier Villars, Paris, (1963), p. 568.
31. M.S. Martin-Gonzalez, A.L. Prieto, R. Gronsky, T. Sands and A.M. Stacy, *J. Electrochem. Soc.*, 149 (2002) C546.

32. W.B. Gosney, *Principles of Refrigeration*; Chap 1, Cambridge University, Cambridge, U.K. (1982).
33. L.D. Hicks, T.C. Harman, X. Sun, and M.S. Dresselhaus, *Phys. Rev. B*, 53 (1996) 10493.
34. B. Y. Yoo, C. K. Huang, J. R. Lim, J. Herman, M. A. Ryan, J. P. Fleurial and N. V. Myung, *Electrochim. Acta*, 50 (2005) 4371.
35. W.J. Danaher and L.E. Lyons, *Aust. J. Chem.*, 37 (1984) 689.
36. Y. Ma, A. Johansson, E. Ahlberg, and A.E.C. Palmqvist, *Electrochim. Acta*, 55 (2010) 4610.
37. H. J. Song, C. C. Liu, J. K. Xu, Q. L. Jiang and H. Shi, *RSC Adv.*, 3 (2013) 22065.
38. P. L. Anto, C. Y. Panicker, H. T. Varghese and D. Philip, *J. Raman Spectrosc.*, 37 (2006) 1265.
39. J. M. Jian, X. S. Guo, L. W. Lin, Q. Cai, J. Cheng and J. P. Li, *Sens. Actuators B*, 178 (2013) 279.
40. S. J. Park, J. An, R. D. Piner, I. Jung, D. X. Yang, A. Velamakanni, S. T. Nguyen and R. S. Ruoff, *Chem. Mater.*, 20 (2008) 6592.
41. L. Q. Qin, S. M. Zhang, J. K. Xu, B. Y. Lu, X. M. Duan and D. H. Zhu, *Int. J. Electrochem Sci.*, 8 (2013) 5299.
42. D. Kim, Y. Kim, K. Choi, J. C. Grunlan and C. Yu, *ACS Nano*, 4 (2010) 513.
43. G. P. Moriarty, S. De, P. J. King, U. Khan, M. Via, J. A. King, J. N. Coleman and J. C. Grunlan, *J. Polym. Sci. Part B: Polym. Phys.*, 51 (2013) 119.
44. K. C. See, J. P. Feser, C. E. Chen, A. Majumdar, J. J. Urban and R. A. Segalman, *Nano Lett.*, 10 (2010) 4664.
45. B. Zhang, J. Sun, H. E. Katz, F. Fang and R. L. Opila, *ACS Appl. Mater. Interfaces*, 2 (2010) 3170.
46. H. J. Song, C. C. Liu, H. F. Zhu, F. F. Kong, B. Y. Lu, J. K. Xu, J. M. Wang and F. Zhao, *J. Electron. Mater.*, 42 (2013) 1268.
47. Y. X. Zhao, J. S. Dyck, B. M. Hernandez and C. Burda, *J. Phys. Chem. C*, 114 (2010) 11607.
48. M. R Dirmyer, J. Martin, G. S. Nolas, A. Sen, J. V. Badding, *Small*, 5 (2009) 933.
49. C. Z. Meng, C. H. Liu and S. S. Fan, *Adv. Mater.*, 22 (2010) 535.
50. Q. L. Jiang, C. C. Liu, J. K. Xu, B. Y. Lu, H. J. Song, H. Shi, Y. Y. Yao and L. Zhang, *J. Polym. Sci. Part B: Polym. Phys.*, 52 (2014) 737.
51. P. Cotterill and P. R. Mould, Recrystallization and Grain Growth in Metals, Wiley: New York, (1976).